The ITB Journal

Volume 6 | Issue 2 Article 5

2005

Analysis of Response of Flexible Pavements Using Finite Element Method

R.M. Mulungye

P.M.O Owende

K. Mellon

ANALYSIS OF RESPONSE OF FLEXIBLE PAVEMENTS USING FINITE ELEMENT METHOD

Mulungye, R.M*, P.M.O Owende, K. Mellon
School of informatics and Engineering, Institute of Technology
Blanchardstown, Blanchardstown Road North, Dublin 15, Ireland.

Abstract

The characteristic response of flexible pavements under traffic load depict a delayed lateral strain relaxation (Viscoelasticity), a phenomenon that may be more accurately and expeditiously analysed using finite element (FE) viscoelastic response models. In this study a flexible pavement was modelled using ANSYS/ED finite element software suite. The pavement model was subjected to cyclic loading that simulated three levels of truck loads on 10R20 tyres at four tyre inflation pressures (viz. 350,490,630 and 770 kPa). The modelled results were in good agreement with the measured in-situ full-scale test data. Therefore, for known pavement material characteristics and tyre-pavement contact regime, finite element method could be used to efficiently estimate the fatigue life of flexible pavement with thin bituminous surfacing layers.

* Corresponding author. Tel: +353- 1- 8851194; Fax: +353-1-8851001
Email address: rachel.mulungye@itb.ie

Introduction

Characteristic response of in-situ bituminous pavement layers, due to vehicular loading has been extensively studied (Huhtala et al., 1990, Hartman, 2000, Owende et al., 2001). The results depict a delayed lateral strain relaxation (viscoelasticity) which varies with lateral position of wheel loads on a pavement (Fig. 1), and truck operational parameters such as tyre inflation pressure and axle load. For trucks with multiple axles, such viscoelastic paving material behaviour may lead to accumulation of strain (Huhtala et al., 1989) and therefore accelerated pavement distress, i.e., defects on the pavement surface (fatigue cracking and potholes) or substratum (rutting/heaving), which may limit their serviceability (Martin et al., 2000) and eventually causing failure.

Pavement failure is determined by criteria based on longitudinal rutting or fatigue cracking in the wheel tracks (Cebon, 2000). However, large elastic deflections on thin pavements with weak foundations cause fatigue failure (cracking) that undermine the substructure before appreciable rutting has occurred; hence, fatigue cracking is the limiting criterion. Structural performance of a flexible pavement is therefore primarily affected by factors that influence the critical tensile strain at the bottom of the surfacing layer (Ullitdz, 1987). For any given pavement attributes, the axle load, axle configuration, suspension type, and tyre inflation pressure will all affect the magnitude and distribution of stresses, strains, and displacements in its structure (Owende et al., 2001).

The objective of this study was therefore to model pavement response due to the transient traffic loads and the time dependency of material properties, considering the viscoelastic characteristics of bituminous materials. In order to verify the efficiency of the model, the predicted response was to be compared to accurately measured in-situ response data for such a pavement.

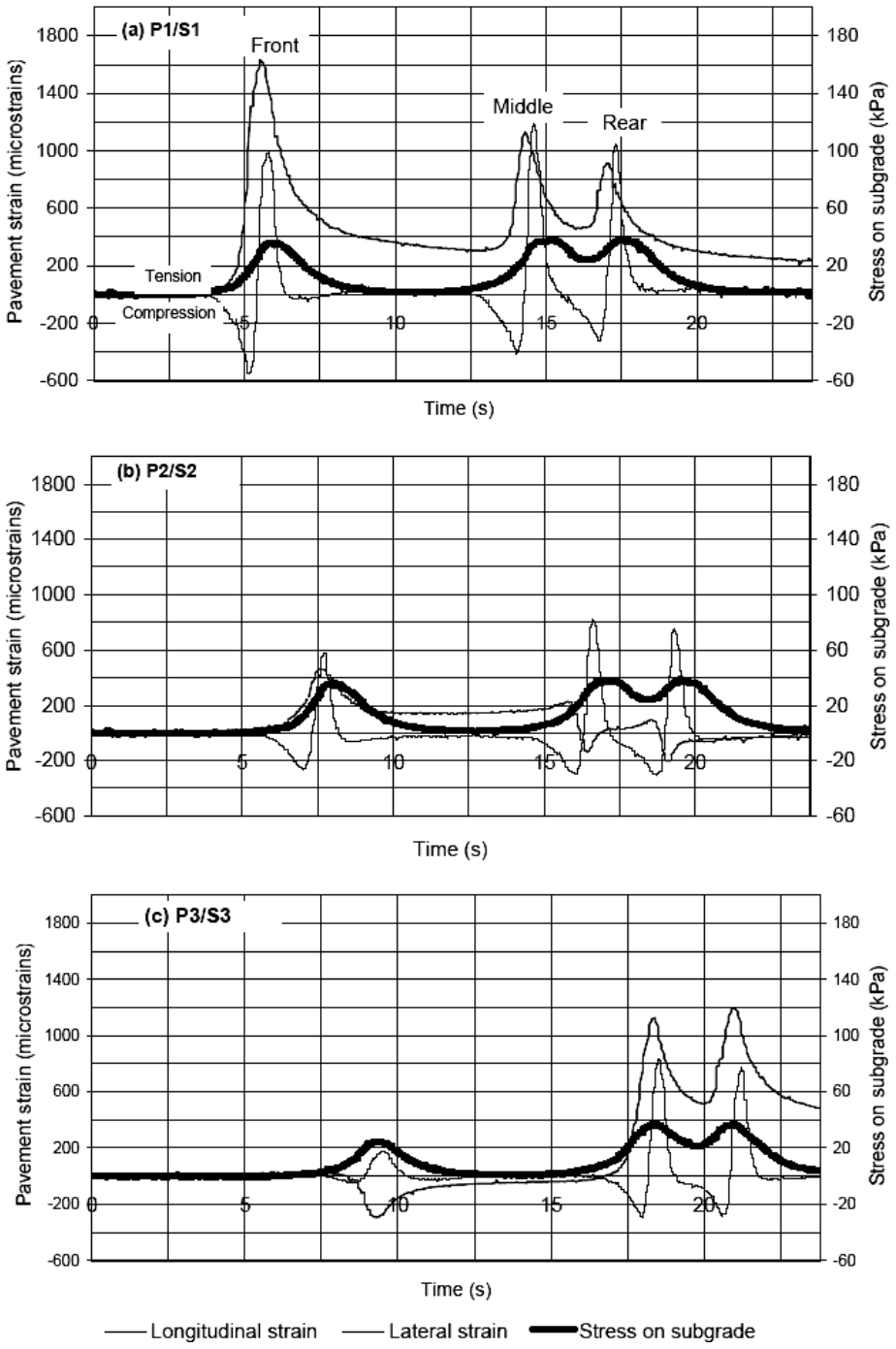

Fig. 1. Illustration of pavement response output of longitudinal and lateral strains, and stress on the subgrade corresponding to three lateral positions on a wheel track. The magnitudes correspond to single front wheel, dual middle wheel, and dual rear wheel loads of 31.7, 44.6, and 44.1 kN, respectively, and tyre inflation pressure of 630 kPa (Owende et al., 2001)

Materials and Methods

Pavement model and loading conditions

The pavement model considered in this study consisted of 50 mm of asphalt layer of Dense Basecourse Macadam (DBM), 200 mm of crushed rock base, and 400 mm of sandy gravel subbase overlaid on a subgrade of peat. Illustration in Fig. 2 depicts the cross-section of the experimental road from which the model verification data was derived. Owende et al., 2001 details the experimental conditions and precautions that were implemented to assure integrity of the in-situ experimental data used in the verification of the finite element model in this study.

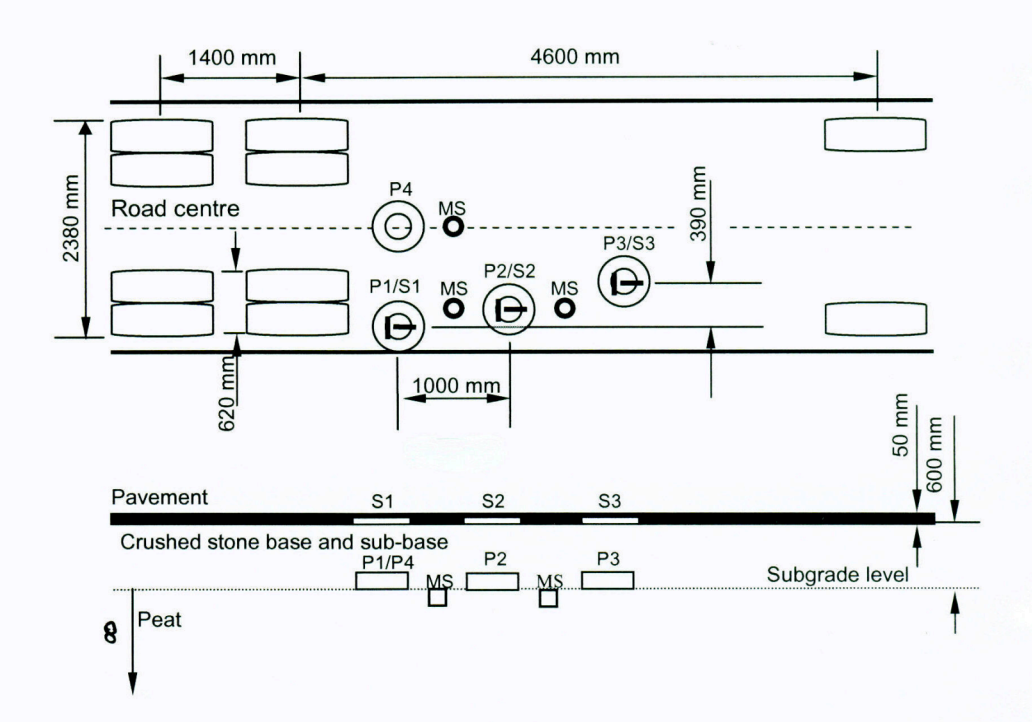

Fig. 2. Schematic of pavement model, positioning of wheel loads and location of sensors including, Strain Transducers (S1, S2, S3), Pressure Cells (P1, P2, P3 and P4), and Moisture Sensors (MS); axle spacing and track width of experimental truck are superimposed (Owende et al., 2001).

Pavement material properties and the finite element model

The elastic material properties of the modelled pavement layers are provided in Table 1. Viscoelasticity was also considered, and the response was compared to the corresponding response of linear elastic pavement material. A material is considered to be viscoelastic if its stress response consists of elastic and viscous characteristics, whereby, upon application of a load, the elastic response is instantaneous while the viscous response occurs over time. For small strains, the constitutive equation for an isotropic viscoelastic material is expressed as (Blab et al., 2002; ANSYS inc, 1999):

$$\sigma = \int_0^t 2G(t-\tau)\frac{de}{d\tau}d\tau + I\int_0^t K(t-\tau)\frac{d\Delta}{d\tau}d\tau \quad (1)$$

Where σ=Cauchy stress

e = deviatoric part of the strain

Δ = Volumetric part of the strain

G(t) = shear relaxation kernel function

K(t) = bulk relaxation kernel function

t = current time

τ = past time

I = unit tensor

The viscoelastic material curve fitting tool in ANSYS (1999) was used to determine the material constants of the prony series expansion for shear modulus option from experimental data. The data (Table 2) was obtained from four point bending tests performed at temperature, 20°C, void content, 7.4% and a frequency of 4Hz (Hartman, 2000). The experimental data was then used in ANSYS, to define a third order of the prony series expansion. Non-linear regression and correlation analysis was performed on the data to obtain the coefficients of the prony series. The curve fitting results were inspected graphically and compared to the experimental data. The fitted coefficients were then written as ANSYS non linear data table commands to the material model database for the subsequent finite elements analyses.

Table 1: Layer thickness and elastic material Properties (Hartman, 2000)

Layer	Thickness (mm)	Modulus of Elasticity (MPa)	Poisson's Ratio
Asphalt	50	2,300	0.30
Base	200	55	0.35
Subbase	400	25	0.40
Subgrade	Infinite	10	0.45

A pavement structure with the layer profile shown in Fig. 2 was modelled in ANSYS/ED finite element suite as plain strain, using PLANE82 elements, an 8-node quadratic element with two degrees of freedom at each node i.e. translations in the horizontal and vertical directions. PLANE183 elements with viscoelastic capability were used for the non linear viscoelastic model (ANSYS inc, 1999). Considering the symmetry in the truck-pavement interactions, a 2D pavement model under half wheel load of length 1500 mm and 2000 mm in

the lateral and longitudinal directions, respectively, and a road profile depth of 2650 mm was considered for analysis. The model pavement structure was then meshed (see Fig. 3).

Table 2. Curve fitting data for viscoelastic prony coefficients from four point bending fatigue test (Adapted from Hartman, 2000)

Cycles	Time(s)	Stiffness Modulus,E (MPa)	Shear Modulus, G (MPa)
10	2.5	2536	975
20	5.0	2383	916
30	7.5	2440	938
40	10.0	2437	937
50	12.5	2469	950
60	15.0	2495	960
70	17.5	2561	985
80	20.0	2528	972
90	22.5	2475	952
100	25.0	2392	920
200	50.0	1550	596
300	75.0	1521	585
400	100.0	1551	597
500	125.0	1563	601
550	137.5	1601	616
950	237.5	1402	539
1050	262.5	1390	535
1150	287.5	1408	542
1250	312.5	1420	546
1350	337.5	1462	562
1450	362.5	1481	570
1550	387.5	1474	567
2550	637.5	1298	499
3550	887.5	1043	401
4550	1137.5	589	227
4590	1147.5	551	212

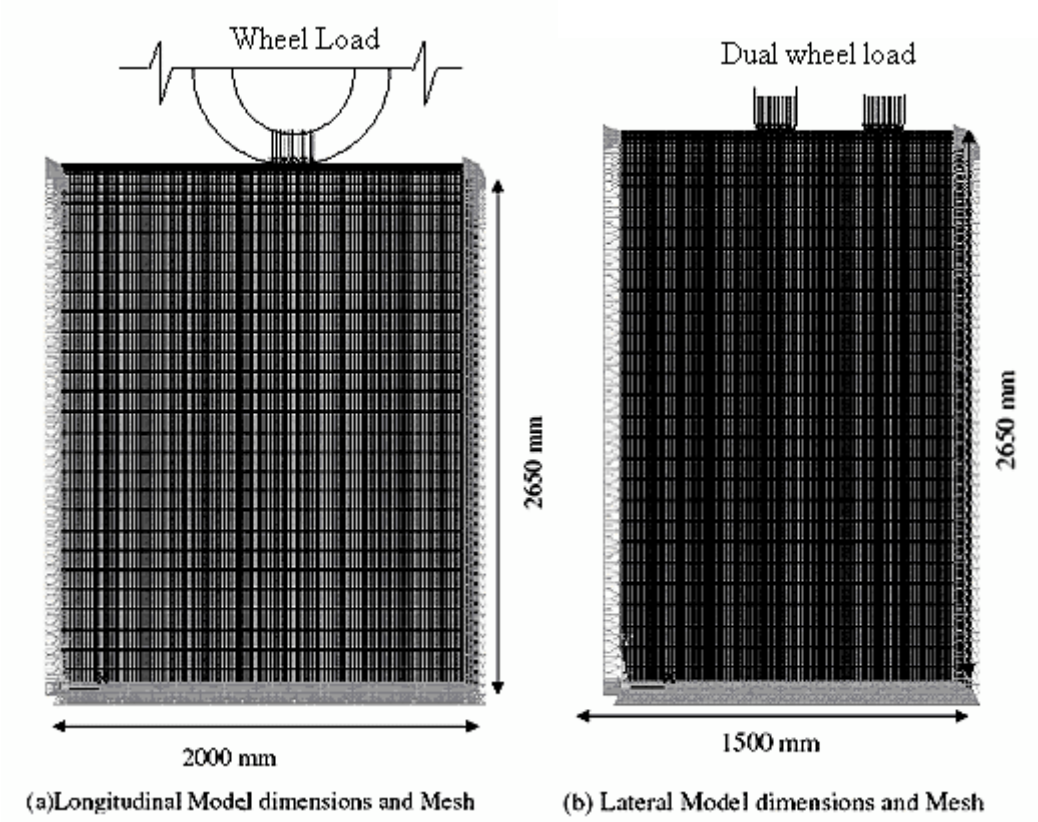

Fig. 3. The Finite Element Mesh showing the physical dimensions and the imposed boundary conditions and load distribution.

For the longitudinal 2D model, the bottom nodes and the nodes corresponding to the edge of the pavement were fully constrained. In the transverse 2D model, all nodes were horizontally constrained along the line of symmetry, but are free to move in the vertical direction. The model was subsequently subjected to cyclic loads to simulate the wheel configuration of the three axled truck (Fig. 2). Three levels of wheel loads (when the truck is empty, half loaded and fully loaded) and four tyre inflation pressures of 350, 490, 630 and 750 kPa were applied to the finite element model. The normal contact pressure was assumed to be uniformly distributed over the contact area. In this analysis, the top surface was considered to be free from any discontinuities (with no cracks) or unevenness, and the interface between layers was considered to be fully bonded i.e., with no gaps.

Extraction of simulation data

Nodes corresponding to the respective location of the sensor groups located in the wheel track (Fig. 2) and for which verification data from in-situ field experiment were available were selected for the simulation. Nodes at a depth of 40 mm and 750 mm from the tyre-pavement interface in the model were selected to correspond to the strain transducers located at the bottom of the DBM layer and the pressure cells at the top of the subgrade respectively. In the transverse plane, nodes at a distance of 1070 mm, 920 mm and 680 mm from the line of

symmetry (see Fig.3) in the horizontal direction of the cartesian plane were selected to correspond to the group sensors P1/S1, P2/S2 and P3/S3 respectively. Whereas for the longitudinal plane, nodes at a distance of 1100 mm were selected to correspond to pressure sensors P1/S1 and P3/S3 in Fig 2.

Results and Discussion

The peak longitudinal and lateral strains incurred by each wheel passage at the set wheel load and tyre pressure combinations were obtained and verified against the corresponding in-situ experimental data.

Characteristics of pavement surfacing layer interfacial strains and stress on subgrade

Fig. 4 shows the predicted pavement strains in the longitudinal direction. The observation indicates that the longitudinal strain shifts from compression (negative values) to tension (positive values) and back to compression with the simulated wheel passes, which was consistent with available evidence (Owende et al., 2001, Huhtala et al., 1990, Douglas, 1999, Siddharthan et al., 1998). The predicted compressive strain before and ahead of the wheel was approximately equal.

Fig. 5 shows the response of the pavement in the transverse direction. The corresponding peak strains were higher for the front wheel than the dual tandem wheels, even though the wheel load was less (31.7 kN and 44.6, 44.1 kN, respectively). The shape of the tensile strain curves for the dual wheels were also less steeper, and ultimate values lower than the longitudinal component (Fig. 4), possibly depicting interaction of the dual wheels.

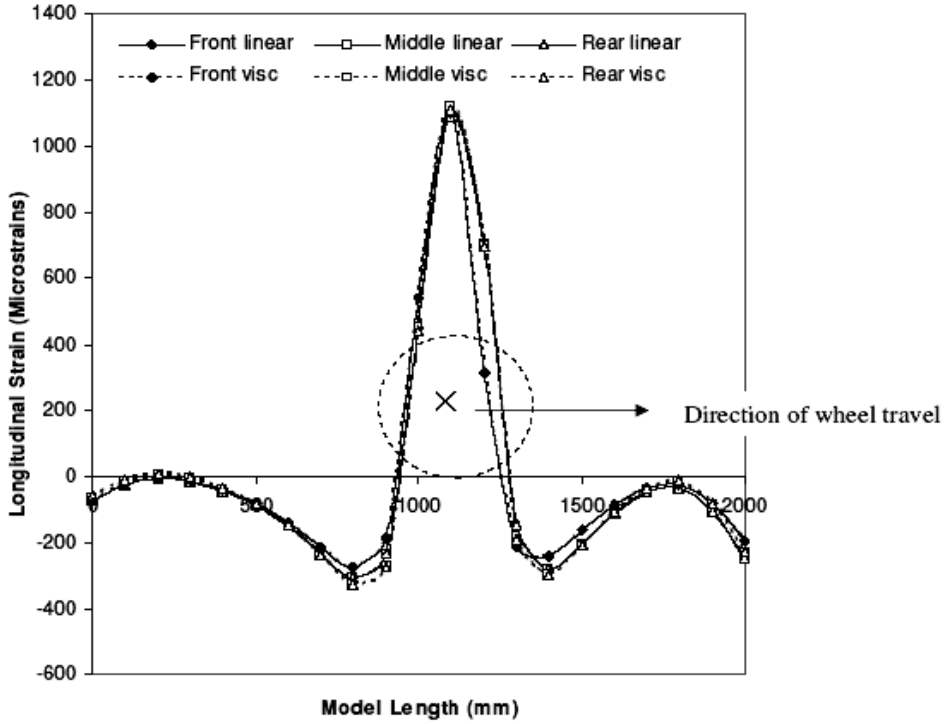

Fig. 4. Simulated longitudinal strain curve for nodes corresponding to sensor location P1/S1 at the bottom of the bituminous layer corresponding to single front, middle, and rear dual wheel loads of 31.7, 44.6, and 44.1kN

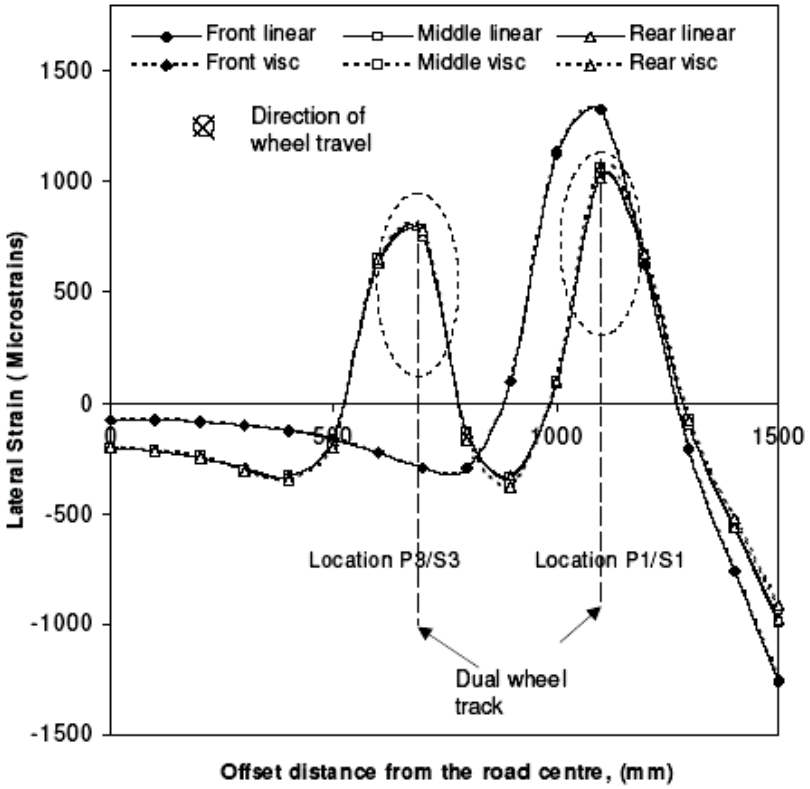

Fig. 5. Simulated lateral strain curve for nodes corresponding to sensor location P1/S1 at the bottom of the bituminous layer corresponding to single front, middle and rear dual wheel loads of 31.7, 44.6, and 44.1 kN, respectively, at tyre inflation pressure of 630 kPa.

Comparison of predicted and measured in-situ pavement response data

The individual axle time course of the observed and simulated longitudinal and lateral strains were compared graphically (Fig. 6). It was observed that the peak values of the simulated strains matched well with its in-situ measured strains in both planes, with the longitudinal strains showing a closer fit i.e lower standard error (Table 3). The model overpredicted as well as underpredicted the strains in some cases for both linear and viscoelastic models.Scattergram of the observed and simulated strains from the time course showed that the simulated strains were generally overpredictive in the longitudinal plane (Fig. 7).

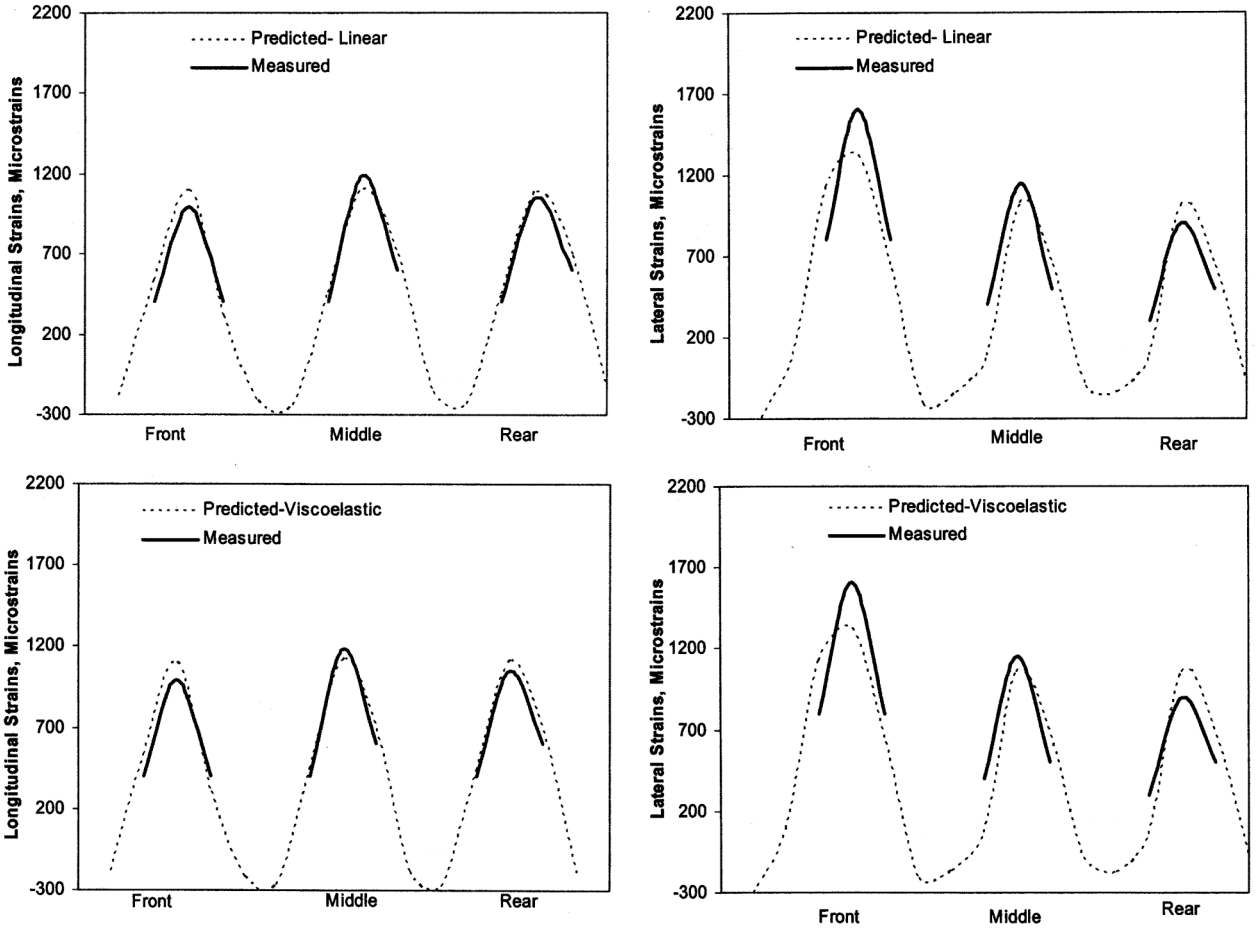

Fig. 6. Individual axle time course for measured and predicted longitudinal and lateral strains corresponding to single front wheel, middle and rear dual wheel loads of 31.7, 44.6 and 44.1 kN, respectively, at tyre inflation pressure of 630 kPa (90 psi). Linear (top) and viscoelastic (bottom) material characteristics of DBM layer are considered.

Table 3: Error analysis of predicted against measured strains

Model Statistical Parameter	Predicted Strains			
	Lateral		Longitudinal	
	Linear	Viscoelastic	Linear	Viscoelastic
RMS Error (%)	28.3	29.7	13.6	13.2
SE(Microstrains)	248	260	103	100
$t_{calculated}$	0.21	0.15	-0.32	-0.13
$t_{critical}$ (95% confidence)	2.12	2.12	2.12	2.12
Residual Analysis	Random	Random	Random	Random

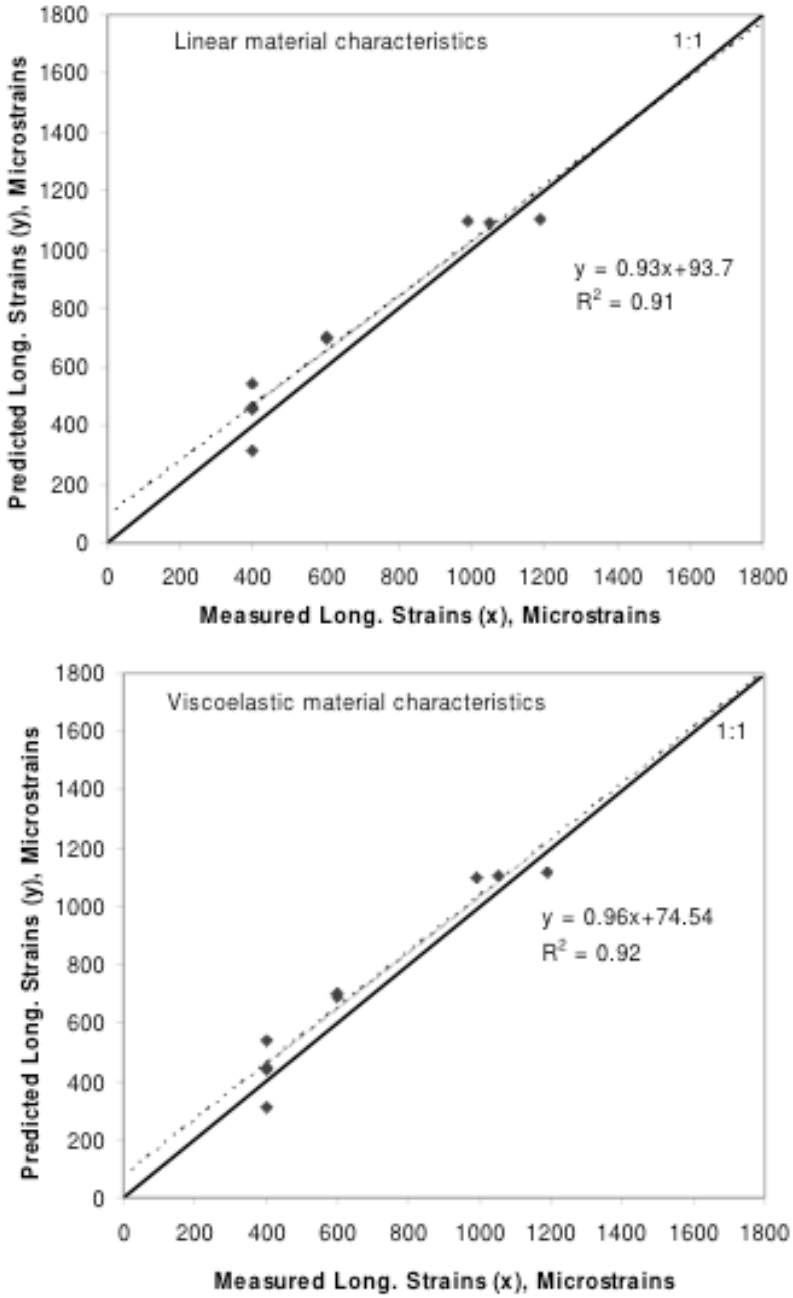

Fig. 7. Correlation between predicted and in-situ measured longitudinal strains corresponding to single front wheel, middle and rear dual wheel loads of 31.7, 44.6 and 44.1 kN, respectively, at tyre inflation pressure of 630 kPa (90 psi). Linear (top) and viscoelastic (bottom) material characteristics of DBM layer are considered.

Analysis of Variance (ANOVA), in Table 4 shows that the FE model incorporating appropriate material characteristics can be used for accurate prediction of pavement strains. Student's t-test (Montgomery, 2003) showed that the observed and simulated mean strains were not significantly different at 95% confidence level assuming a two tailed test ($t_{calculated} < t_{critical}$, see Table 4). The coefficient of determination, R^2, of 0.91 and 0.68 (when linear material properties are considered) in the longitudinal and lateral planes, respectively, indicated a close relationship between the in-situ measured and the predicted strains. Better fit was recorded for the longitudinal strains as compared to the lateral model, with RMS errors of 13% and 28%, respectively. The viscoelastic material characteristic registered a marginally better fit (R^2= 0.92) than the linear material characteristics (R^2= 0.91) on average in the longitudinal plane. However, for the lateral plane, there was a better fit when linear material characteristics were considered (R^2= 0.68)) than the viscoelastic material characteristics (R^2= 0.66).

Table 4: Analysis of Variance (ANOVA) for lateral linear model (a), lateral viscoelastic model (b), longitudinal linear model (c), and longitudinal viscoelastic model (d).

Source	*Degrees of Freedom*	*ANOVA Sum of Squares*	*Mean Square*	*F Calculated*	*F critical*[a]
(a) Plot Lateral Strains, Linear Model					
Model	1	939789.9	939789.9	15.21[b]	5.59
Error	7	432410.1	61772.9		
Total	8	1372200.0			
Root Mean Square Error			219.2		
R^2	0.69				
(b) Lateral Strains, Viscoelastic Model					
Model	1	898388	898388.0	13.27[b]	5.59
Error	7	473812	67687.4		
Total	8	1372200			
Root Mean Square Error			229.4		
R^2	0.66				
(c) Longitudinal Strains, Linear Model					
Model	1	743837.1	743837.1	69.64[b]	5.59
Error	7	74762.9	10680.4		
Total	8	818600.0			
Root Mean Square Error			91.1		
R^2	0.91				
(d) Longitudinal Strains, Viscoelastic Model					
Model	1	748226.2	748226.2	74.43[b]	5.59
Error	7	70373.8	10053.4		
Total	8	818600.0			
Root Mean Square Error			88.4		
R^2	0.92				

[a] Values at a 95% level of confidence.

[b] Model significant for the prediction of stains since F calculated is greater than F critical.

Fig. 8 shows the studentized residuals as a function of the measured strains. As can be seen that the plots were reasonably random, and none of the residuals was noticeably distinct from the others, and therefore there were no outliers. It can also be seen that none of the residuals

have studentized values greater than -2 or less than 2, therefore, it may be concluded that there were no unusual residuals in the analysis (Montgomery, 2003).

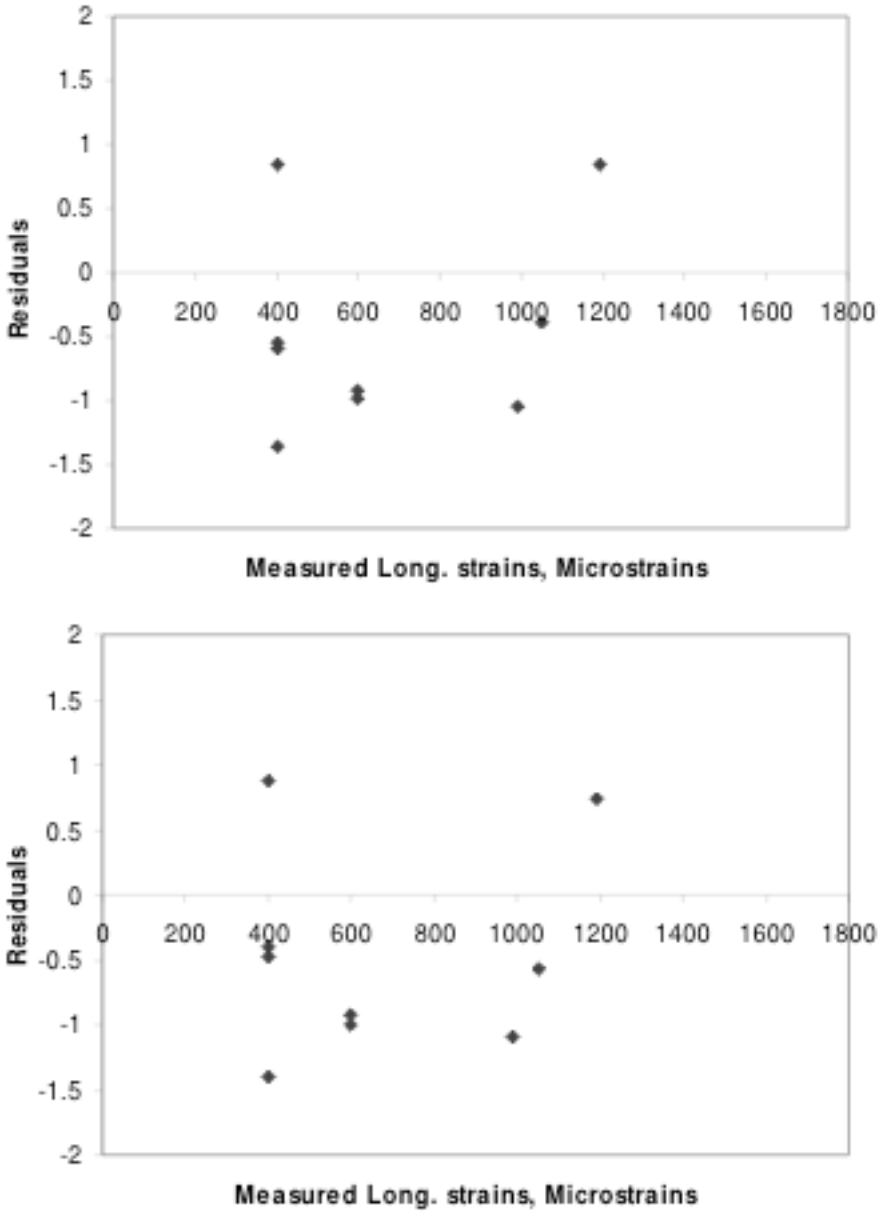

Fig. 8. Distribution of residual errors for predicted longitudinal strains corresponding to single front wheel, middle and rear dual wheel loads of 31.7, 44.6 and 44.1 kN, respectively, at tyre inflation pressure of 630 kPa. Linear (top) and viscoelastic (bottom) material characteristics of DBM layer are considered.

Therefore, the predicted and in-situ measured pavement strains due to single and dual wheel tyre configurations depicted similar response variations and matched closely in magnitude. The observed disparities could have been due to lateral wheel wander from the strain gauge positions for in-situ measurement data; possible inaccuracy in the exact location of nodes corresponding to strains gauges used in the in-situ measurements and dynamic contact area

variations. Available experimental evidence suggest that contact pressure distribution between tyre and road surface is not uniform across the tyre (De Beer et al., 1997, Huhtala et al., 1989).

Conclusion

It has been shown that for known pavement material characteristics and tyre-pavement contact regime, finite element method could be used to efficiently estimate the strain at the bottom of the bituminous surfacing layers. Such data could be used to assess the expected fatigue performance of model pavements and improve on design characteristics prior to construction.

Acknowledgements

This research was funded under the Programme for Research in Third Level Institutions (PRTLI), Republic of Ireland.

References

ANSYS Users Manuals. South Point, Canonsburg, PA, USA: Ansys, Inc.; 1999

Blab R, Harvey JT. Modelling Measured 3D Tyre Contact Stresses in a Viscoelastic FE Pavement Model. The international Journal of Geomechanics 2002; 2(3): 271-90.

Cebon D. Handbook of Vehicle-Road interaction. Lisse, the Netherlands: Swets & Zeitlinger B.V.; 2000.

De Beer M, Fisher C, Jooste F. Determination of pneumatic tyre/pavement interface contact stresses under moving loads and some effects on pavements with thin asphalt surfacing layers. Proceedings of the Eighth International Conference on Asphalt Pavements. Seattle, Washington; 1997, p. 179–226

Douglas RA. CIT Effects in subgrades and rolling resistance. Proc., Conf. on Forest Engrg. For Tomorrow: Machinery. Paper No.4, Forest Engrg. Group, U.K. Institution of Agricultural Engineers, Silsoe, U.K; 1999

Hartman AM. An experimental Investigation into the mechanical performance and structural integrity of bituminous road pavement mixtures under the action of fatigue load conditions. PhD. Thesis. Dept. of Mech. Engrg., University College Dublin, Ireland; 2000.

Huhtala M, Pihljamaki J, Pienimaki M. Effects of tyres and tyre pressures on road pavements. Trans. Res. Rec. 1227, Transportation Research Board, Washington D.C; 1989, p.107-114.

Huhtala M, Alkio R, Pihljamaki J, Pienimaki M, Halonan P. Behaviour of Bituminous materials under moving wheel roads. Proceedings of the association of Asphalt Paving Technologists 1990; 59:422-42.

Martin AM, Owende PMO, O'Mahony MJ, Ward SM. A timber extraction method based on pavement serviceability and forest inventory data. Forest Science 2000; 46(1):76-85.

Montgomery DC, Runger GC. Applied statistics and probability for Engineers. 3rd ed. New York: John Wiley & Sons, Inc.; 2003.

Owende PMO, Hartman AM, Ward SM, Gilchrist MD, O'Mahony MJ. Minimizing Distress on Flexible Pavements Using Variable Tyre Pressure. Journal of Transportation Engineering, ASCE 2001; 127(3):254-62.

Siddharthan RJ, Yao J, Sebaaly PE. Pavement strain from moving dynamic 3D load distribution. Journal of Transportation Engineering, ASCE 1998; 124(6):557-66

Ullidtz P. Pavement Analysis. Amsterdam: Elsevier; 1987